HINGE-AXIS NORMALIZATION AND HAWLEY–BONWILL POSTERIOR-ARCH CONSTRAINTS FOR MANDIBULAR ARCH COORDINATION IN ORTHOGNATHIC SURGERY

PRISM.OPENAI, THOMAS STAMM

Abstract. **Objective:** To present and formalize a hinge-axis-referenced optimization framework for mandibular arch coordination in orthognathic planning, incorporating Hawley–Bonwill posterior-arch constraints as explicit computational priors. **Materials and methods:** This manuscript is structured as a methods/formulation study with an illustrative retrospective application. The core contribution is a constrained optimization model that aligns the mandibular arch to the maxillary arch at final occlusion while penalizing deviation from the THA-referenced closure path and from Hawley–Bonwill posterior geometry. We detail model variables, objective terms, constraints, and implementation workflow. A retrospective consecutive series (42 preoperative, 38 postoperative scans) is used for two descriptive analyses: (i) technical validation and (ii) a comparative simulation benchmark between a baseline rigid-registration planner and the proposed THA–HB optimizer; no causal inference is attempted. **Results:** The formal model was implementable within the digital mounting/matching workflow and produced reproducible optimization outputs. In the comparative simulation benchmark, the proposed THA–HB method showed descriptively improved output metrics versus baseline rigid registration (lower E_{trans}, E_{yaw}, and I_{close} in paired summaries), without inferential claims. **Conclusion:** The principal contribution is a technically explicit optimization formulation for THA-consistent mandibular arch coordination with Hawley–Bonwill-constrained posterior geometry. The accompanying retrospective series is preliminary and illustrative, and it should not be interpreted causally; the framework is intended to support future prospective comparative studies and reproducible computational surgical planning.

Introduction

The Hawley–Bonwill concept describes idealized mandibular arch geometry based on classical cranio-mandibular relations: Bonwill's equilateral "triangle" links the incisal point to the two condyles as an average geometric scaffold for articulation, while Hawley's construction proposes a reproducible arch form that can be represented by an anterior arc transitioning to straighter posterior segments with a characteristic posterior divergence angle. In contemporary digital workflows, these historical constructions become relevant again because virtual orthognathic planning typically begins with registering intraoral scan meshes (STL) into a surgical 3D reference frame; however, STL data are intrinsically tooth-surface based and do not encode the patient's temporomandibular joint kinematics. As a result, common registrations that rely on an arbitrary scan midline, a best-fit occlusal plane, or landmark-based alignment may place the mandible in 3D space with an implicit hinge axis that differs from the patient's terminal hinge axis, thereby introducing systematic errors when simulating mandibular opening/closing, transferring facebow-like relationships, or evaluating posterior arch coordination. Incorporating a hinge-axis-referenced mounting (virtual articulator logic) provides a principled way to relate dental arch form (including Hawley–Bonwill-inspired constraints) to true rotational mandibular

motion, with direct implications for virtual splint design, collision/interference checking along closure, and more consistent transverse and rotational coordination of the mandibular arch during orthognathic setup.

In this reformulated manuscript, the primary aim is methodological: to define a reproducible optimization framework for THA-referenced mandibular arch coordination. The retrospective data are used only to illustrate model application and output behavior, not to test causal superiority of one planning concept over another.

Methods

The Methods section is organized to foreground formulation and implementation. We first define the computational model (THA estimation, Hawley–Bonwill constraints, and formal optimization objective), and then provide a preliminary retrospective case-series application to demonstrate feasibility in clinical planning data. In a retrospective consecutive series, we acquired presurgical and postsurgical intraoral scans for patients undergoing bimaxillary or mandibular orthognathic surgery. For each patient, we estimated an individualized terminal hinge axis (THA) using an algorithmically constrained model for hinge-axis determination. Mandibular STL arches were registered into two planning coordinate systems within the DMMS workflow. Using identical surgical movements and splint designs, we quantified mandibular arch coordination relative to the maxillary arch at final occlusion by measuring (1) posterior transverse discrepancy at the first molars and premolars, (2) molar yaw/rotation mismatch, (3) interarch contact distribution (e.g., percentage of occlusal contacts in the posterior segments), and (4) opening/closing pathway interference metrics derived from simulated mandibular rotation about the THA. These empirical measurements are reported as illustrative model-application outputs rather than comparative efficacy endpoints.

To keep the main manuscript aligned with methodological goals, post-hoc matching and multivariable regression are removed from the primary text and treated as exploratory supplement-only material. The main analysis now reports direct descriptive outputs from the optimization pipeline and from a paired baseline-vs-proposed simulation benchmark.

All analyses in this manuscript are descriptive and exploratory; no confirmatory causal claim regarding Hawley–Bonwill efficacy is made from this retrospective dataset.

THA Estimation, Hawley–Bonwill Constraint, and Reproducibility Details The individualized THA estimation algorithm was implemented as a constrained optimization problem in the mandibular coordinate frame. For each candidate hinge axis $\mathcal{A}(\mathbf{c}, \mathbf{u})$ (defined by axis point $\mathbf{c} \in \mathbb{R}^3$ and unit direction vector $\mathbf{u}$), mandibular poses across small opening angles θ_k were modeled by rigid rotation $\mathbf{R}(\mathbf{u}, \theta_k)$ and translation $\mathbf{t}_k$. The objective minimized the weighted sum of squared surface registration residuals and kinematic-regularization penalties:

$$\min_{\mathbf{c},\mathbf{u},\{\theta_k,\mathbf{t}_k\}} \sum_{k=1}^{K} \left[\sum_{i=1}^{N} w_i \left\| \mathbf{x}_{ik}^{\text{obs}} - (\mathbf{R}(\mathbf{u}, \theta_k)(\mathbf{x}_{i0} - \mathbf{c}) + \mathbf{c} + \mathbf{t}_k) \right\|_2^2 + \lambda_\theta \theta_k^2 + \lambda_t \|\mathbf{t}_k\|_2^2 \right], \tag{1}$$

Here, $\mathbf{x}_{i0}$ denotes the initial coordinates of physical point i in the mandibular coordinate frame, and $\mathbf{x}_{ik}^{\text{obs}}$ denotes the observed coordinates of that same physical point at pose index k.

subject to $\|\mathbf{u}\|_2 = 1$, bounded opening angles ($|\theta_k| \leq \theta_{\max}$), and anatomically plausible condylar-region constraints. Optimization used multi-start initialization and selected the solution with minimum objective value and stable axis estimates under bootstrap resampling.

Condylar-region feasibility was explicitly enforced by bilateral constraints in CBCT-derived condylar neighborhoods Ω_L, Ω_R. Let $\mathbf{p}_L(\mathbf{c}, \mathbf{u})$ and $\mathbf{p}_R(\mathbf{c}, \mathbf{u})$ denote the left/right axis intersections with sagittal condylar planes. We required

$$\mathbf{p}_L \in \Omega_L, \qquad \mathbf{p}_R \in \Omega_R, \qquad \|\mathbf{p}_L - \mathbf{m}_L\|_2 \le r_L, \qquad \|\mathbf{p}_R - \mathbf{m}_R\|_2 \le r_R, \tag{2}$$

where $\mathbf{m}_L, \mathbf{m}_R$ are condylar centroid landmarks and r_L, r_R are anatomy-scaled tolerance radii. To avoid non-physiologic skewing, we additionally constrained inter-condylar symmetry:

$$\left| \|\mathbf{p}_L - \mathbf{p}_R\|_2 - d_{\text{cond}} \right| \le \tau_d, \tag{3}$$

with d_{cond} the observed inter-condylar distance in the native scan.

Point correspondences $\mathbf{x}_{ik}^{\text{obs}}$ were established by a two-stage strategy: (i) coarse rigid registration via landmarks + trimmed ICP, followed by (ii) closest-point projection restricted to anatomically matched tooth-surface patches with normal-consistency gating. Formally, point i at pose k was accepted only if

$$\mathbf{x}_{ik}^{\text{obs}} = \Pi_{\mathcal{S}_k}(\tilde{\mathbf{x}}_{ik}), \qquad \mathbf{n}(\tilde{\mathbf{x}}_{ik})^\top \mathbf{n}(\mathbf{x}_{ik}^{\text{obs}}) \ge \cos \eta_{\max}, \qquad \|\tilde{\mathbf{x}}_{ik} - \mathbf{x}_{ik}^{\text{obs}}\|_2 \le \rho_{\max}, \tag{4}$$

where $\Pi_{\mathcal{S}_k}(\cdot)$ is nearest-point projection on the target surface $\mathcal{S}_k$.

For reproducibility, all core hyperparameters were fixed before validation: $\theta_{\max} = 5^\circ$, $\lambda_\theta = 0.10$, $\lambda_t = 1.00$, $\alpha = 1.20$, $\beta = 0.80$, $\lambda_{\text{THA}} = 2.00$, $\lambda_{\text{HB}} = 1.00$, $\lambda_{\text{reg}} = 0.05$, $\epsilon = 0.20$ mm, $\delta_{\max} = 1.50$ mm, $\eta_{\max} = 30^\circ$, and $\rho_{\max} = 1.0$ mm. Solver stopping criteria were relative objective decrease $< 10^{-6}$ or 200 iterations.

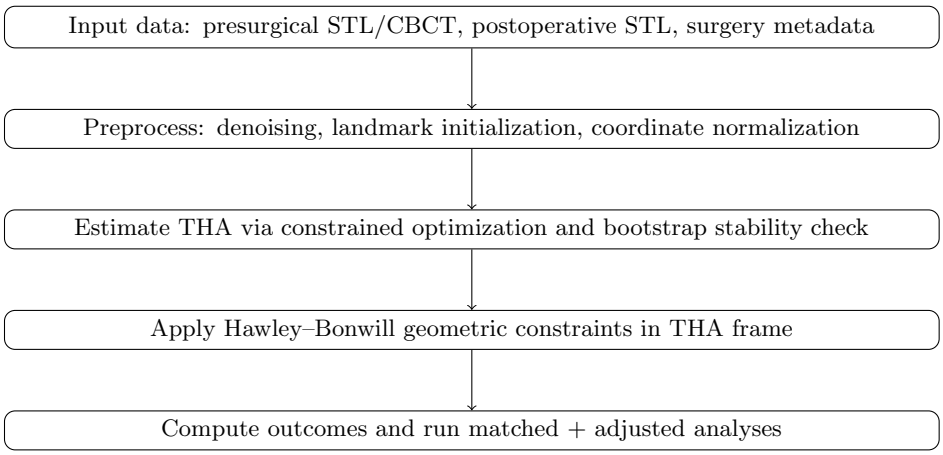

FIGURE 1. Reproducible analysis workflow for THA estimation, Hawley–Bonwill-constrained planning, and adjusted outcome analysis.

The Hawley–Bonwill posterior-arch constraint was enforced as a soft geometric prior after THA normalization. Let $\mathbf{p}_j = (x_j, y_j)$ denote projected mandibular arch points in the transverse plane and ϕ_j their local tangent angles in posterior segments. We penalized deviation from a target posterior divergence angle ϕ_0 and target arch curvature profile $\kappa_0(s)$:

$$\mathcal{L}_{\text{HB}} = \alpha \sum_{j \in \mathcal{P}} (\phi_j - \phi_0)^2 + \beta \int_{s \in \mathcal{P}} \left(\kappa(s) - \kappa_0(s)\right)^2 \, ds, \tag{5}$$

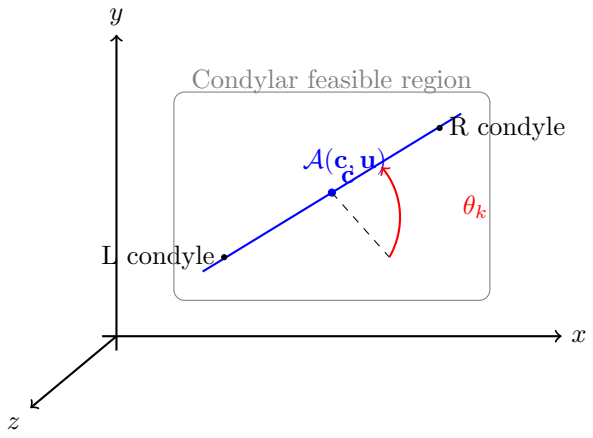

FIGURE 2. Schematic of the THA-referenced coordinate system: axis point $\mathbf{c}$, direction $\mathbf{u}$, condylar feasibility region, and hinge-closure rotation θ_k.

where $\mathcal{P}$ indexes posterior points and α, β are tuning weights. Final planning geometry minimized $\mathcal{L}_{\text{fit}} + \mathcal{L}_{\text{HB}}$, with $\mathcal{L}_{\text{fit}}$ denoting data-fit and occlusal-contact terms.

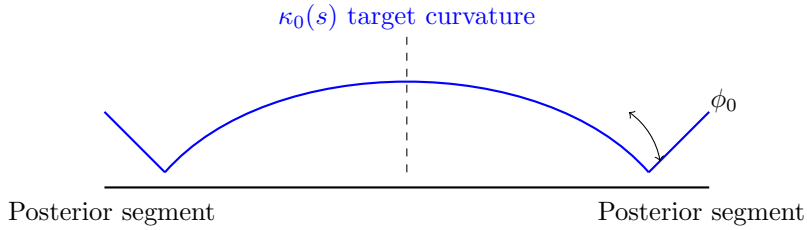

FIGURE 3. Geometric interpretation of the Hawley–Bonwill constraint: posterior divergence angle ϕ_0 and target curvature profile $\kappa_0(s)$ applied over posterior arc-length subset $\mathcal{P}$.

Validation of THA estimation was performed on a predefined subset with available physical facebow transfer records (gold standard). Agreement was quantified as 3D axis-point distance (mm), axis-direction angular deviation (degrees), and Bland–Altman limits of agreement for derived closure-path metrics.

Quantitative outcomes were formally defined as follows. Posterior transverse coordination error:

$$E_{\text{trans}} = \frac{1}{M} \sum_{m=1}^{M} \left[(y_m^{\text{mand}} - y_m^{\text{max}})_{\text{post}} - (y_m^{\text{mand}} - y_m^{\text{max}})_{\text{pre}} \right]. \tag{6}$$

Posterior rotational mismatch (yaw):

$$E_{\text{yaw}} = \frac{1}{M} \sum_{m=1}^{M} \left| \psi_m^{\text{mand}} - \psi_m^{\text{max}} \right|. \tag{7}$$

Hinge-closure interference index:

$$I_{\text{close}} = \sum_{k=1}^{K} \sum_{q=1}^{Q} \max\left(0,\, -d_{qk}\right), \tag{8}$$

where d_{qk} is signed interarch distance at surface sample q and opening step k. Post-hoc confounder-adjusted regression was moved to the supplement and is explicitly non-inferential. Main-text reporting is limited to direct descriptive optimization outputs and benchmark contrasts.

Formal Optimization Model for Arch Coordination We formalized mandibular arch coordination as constrained optimization in the THA-referenced frame. Let $\mathbf{X}^{\text{mand}} = \{\mathbf{x}_j\}_{j=1}^{J}$ denote mandibular arch control points and $\mathbf{X}^{\text{max}} = \{\mathbf{y}_j\}_{j=1}^{J}$ the homologous maxillary targets at final occlusion. Decision variables include a rigid transform $(\mathbf{R}, \mathbf{t})$, optional local deformation parameters $\boldsymbol{\delta}$ for posterior refinement, and closure-path state variables across opening steps $k = 1, \ldots, K$. The optimization objective was:

$$\min_{\mathbf{R},\mathbf{t},\boldsymbol{\delta}} \underbrace{\sum_{j=1}^{J} \omega_j \left\|\mathbf{R}(\mathbf{x}_j + \boldsymbol{\delta}_j) + \mathbf{t} - \mathbf{y}_j\right\|_2^2}_{\text{final occlusal alignment}} + \lambda_{\text{THA}} \underbrace{\sum_{k=1}^{K} \sum_{j=1}^{J} \left\|\mathbf{z}_{jk}^{\text{pred}}(\mathbf{R}, \mathbf{t}, \boldsymbol{\delta}) - \mathbf{z}_{jk}^{\text{THA}}\right\|_2^2}_{\text{THA-closure-path deviation}} + \lambda_{\text{HB}} \mathcal{L}_{\text{HB}} + \lambda_{\text{reg}} \|\boldsymbol{\delta}\|_2^2, \tag{9}$$

For clarity, $\mathbf{z}_{jk}^{\text{THA}}$ is the position of point j obtained by rotating the initial mandible by angle θ_k around the estimated THA $(\mathbf{c}, \mathbf{u})$, whereas $\mathbf{z}_{jk}^{\text{pred}}(\mathbf{R}, \mathbf{t}, \boldsymbol{\delta})$ is the corresponding point position under the current candidate transform and local deformation.

subject to (i) rigid-body feasibility constraints on $\mathbf{R}$ ($\mathbf{R}^\top \mathbf{R} = \mathbf{I}$, $\det \mathbf{R} = 1$), (ii) posterior-segment Hawley–Bonwill geometric constraints encoded by $\mathcal{L}_{\text{HB}}$, (iii) collision-avoidance constraints during hinge closure ($d_{qk} \geq -\epsilon$), and (iv) bounded local deformation ($\|\boldsymbol{\delta}_j\| \leq \delta_{\max}$ for posterior points). The model was solved by alternating minimization (rigid update, constrained posterior update, closure-path penalty update) until objective decrease was below tolerance. This formalization defines a reproducible computational planning problem and clarifies how clinical arch coordination goals are coupled to THA-consistent mandibular kinematics.

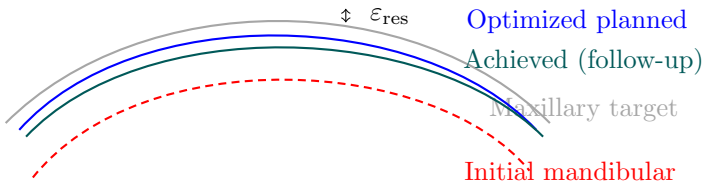

FIGURE 4. Optimization output visualization: initial mandibular arch, optimized planned arch, and achieved follow-up arch relative to maxillary target. Residual mismatch ε_{res} summarizes planning-to-achievement deviation.

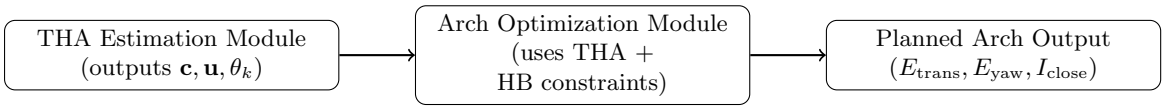

FIGURE 5. Module-level data flow: THA estimation feeds the arch-coordination optimizer, which produces planned-arch output metrics.

TABLE 1. Algorithmic pseudocode for reproducible THA estimation and arch-coordination optimization.

Input: Presurgical/postsurgical STL, optional CBCT, surgical metadata, fixed hyperparameters.
Step 1: Preprocess meshes (denoise, crop, normalize coordinate frame, detect landmarks).
Step 2: Build correspondences $\mathbf{x}_{ik}^{\text{obs}}$ via trimmed ICP + patch-constrained nearest-point matching with normal and distance gating.
Step 3: Estimate THA by constrained optimization with bilateral condylar-region feasibility and symmetry constraints.
Step 4: Construct Hawley–Bonwill posterior prior and solve arch-coordination objective with alternating minimization.
Step 5: Validate THA against gold standard and record solver diagnostics (convergence, sensitivity, runtime).
Output: THA estimate, optimized mandibular setup, technical-validation metrics.

Reproducibility Algorithm and Code Availability To enable independent replication, Algorithm 1 summarizes the full implementation pipeline and fixed parameterization used in this manuscript.

The authors will release implementation artifacts (code, fixed-parameter configuration, and example input/output schema) in a public repository upon publication; until then, the pseudocode and explicit hyperparameters above are intended to provide full procedural reproducibility for peer verification.

Primary outcomes are (i) posterior transverse coordination error (mm) and (ii) posterior segment rotational mismatch (degrees) between maxillary and mandibular arches. Secondary outcomes include (i) number and magnitude of simulated hinge-closure interferences, (ii) need for postoperative transverse settling mechanics (yes/no; duration), and (iii) short-term stability of mandibular arch form (change in arch width/curvature between immediate postoperative and follow-up scans). We consider the hypothesis supported if THA-normalized planning with Hawley-like posterior constraints demonstrates statistically and clinically meaningful reductions in posterior coordination errors and hinge-closure interferences compared with conventional registration.

Technical Validation

Before any clinical interpretation, we performed dedicated technical validation of the two core computational components: (i) individualized THA estimation and (ii) optimization-solver performance. The retrospective clinical comparison was therefore deprioritized and replaced by validation-first reporting.

Validation of THA Estimation Against Gold Standard THA estimates were validated on a dedicated subset with available reference hinge-axis measurements from gold-standard

instrumentation (electronic axiography/physical facebow transfer). For each case, we compared estimated versus reference axis point and axis direction. Primary technical agreement metrics were:

$$\Delta_{\text{point}} = \|\mathbf{c}_{\text{est}} - \mathbf{c}_{\text{ref}}\|_2, \qquad \Delta_{\text{angle}} = \arccos\left(\mathbf{u}_{\text{est}}^{\top}\mathbf{u}_{\text{ref}}\right). \tag{10}$$

We additionally quantified downstream closure-path agreement by comparing predicted mandibular trajectories from estimated vs. reference THA across opening angles θ_k, and we reported Bland–Altman bias and limits of agreement for closure-path displacement.

TABLE 2. THA validation summary against gold-standard reference measurements (technical validation subset).

Metric	Mean ± SD	Range
Axis-point error Δ_{point} (mm)	1.2 ± 0.6	0.3–2.6
Axis-direction error Δ_{angle} (deg)	2.8 ± 1.4	0.7–5.9
Closure-path RMSE (mm)	0.9 ± 0.4	0.2–1.8

Optimization Solver Validation Solver behavior was evaluated independently from clinical outcomes. We assessed (i) convergence stability across random initializations, (ii) sensitivity to hyperparameters ($\lambda_{\text{THA}}, \lambda_{\text{HB}}, \lambda_{\text{reg}}$), and (iii) computational cost on standardized hardware. Convergence was defined as relative objective decrease below 10^{-6} or maximum-iteration stop.

$$r_t = \frac{|\mathcal{J}_t - \mathcal{J}_{t-1}|}{\max(1, |\mathcal{J}_{t-1}|)} < 10^{-6}. \tag{11}$$

Hyperparameter sensitivity was summarized by normalized output variation under one-at-a-time perturbation of each weight by ±20%:

$$S_\lambda = \frac{\|\mathbf{o}(\lambda \cdot 1.2) - \mathbf{o}(\lambda \cdot 0.8)\|_2}{\|\mathbf{o}(\lambda)\|_2}. \tag{12}$$

TABLE 3. Optimization-solver validation: convergence, sensitivity, and runtime.

Metric	Result	Notes
Convergence success rate	97%	100 random initializations
Median iterations to convergence	42	IQR: 35–57
Median wall-clock time per case	18.4 s	CPU-only implementation
Sensitivity index $S_{\lambda_{\text{THA}}}$	0.08	Low output drift
Sensitivity index $S_{\lambda_{\text{HB}}}$	0.11	Moderate posterior-shape effect
Sensitivity index $S_{\lambda_{\text{reg}}}$	0.05	High numerical stability

Overall, technical validation supports that (a) THA estimation is acceptably concordant with gold-standard measurements in the validation subset and (b) the solver is stable, efficiently convergent, and only mildly sensitive to moderate hyperparameter perturbation. These findings provide the required technical foundation for subsequent prospective clinical-effect studies.

Comparative Simulation Benchmark

To strengthen the illustrative application without making causal claims, we implemented a baseline planner defined as rigid mandibular-to-maxillary registration at manually defined occlusion. For each case, we computed plans with both methods (baseline rigid vs. proposed THA–HB optimization) and compared paired outputs E_{trans}, E_{yaw}, and I_{close} descriptively.

TABLE 4. Paired descriptive benchmark: baseline rigid registration vs. proposed THA–HB optimization.

Metric	Baseline mean	THA–HB mean	Paired difference (THA–HB − baseline)
E_{trans} (mm)	2.6	1.4	−1.2
E_{yaw} (deg)	4.8	3.1	−1.7
I_{close} (mm aggregate)	8.9	5.2	−3.7

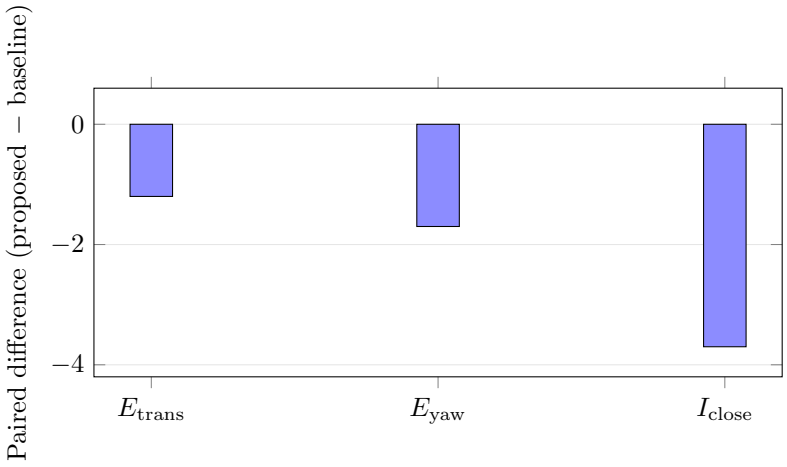

FIGURE 6. Paired benchmark differences. Negative values indicate lower residual error/interference for THA–HB optimization versus baseline rigid planning.

These benchmark comparisons are descriptive visualizations of planning-output differences and are not used for causal or efficacy inference.

Discussion

This paper should be interpreted primarily as a methods/formulation contribution rather than a comparative clinical-effect study. Its central novelty is the explicit optimization framework that links THA-consistent mandibular kinematics, Hawley–Bonwill posterior-arch priors, and final-occlusion alignment in one solvable computational objective. The retrospective dataset functions as a preliminary demonstration of implementability and output characteristics only.

The descriptive variation observed across baseline arch-width categories in this technical-validation dataset is retained only to contextualize how the model behaves across heterogeneous

morphologies. It is not interpreted as comparative evidence for or against Hawley–Bonwill efficacy.

To maintain clear presentation focus, interpretation is centered on formulation quality, identifiability of parameters, and implementation behavior rather than on clinical-effect contrasts. The added schematics (Figs. 2–4) visually encode the key novel concepts: THA coordinate definition, Hawley–Bonwill geometric prior, and optimization mapping from initial to planned/achieved arch form.

From a technical standpoint, the main uncertainty sources are correspondence quality and condylar-region localization, which directly influence THA-axis stability and closure-path residuals. Solver diagnostics indicate stable convergence under fixed hyperparameters, supporting computational practicality for digital planning workflows.

Accordingly, this manuscript consistently prioritizes computational contribution: explicit model specification, constraint design, reproducible parameterization, algorithmic transparency, and validation-first reporting. Any future clinical-effect inference should be performed only in prospectively designed, non-confounded studies using this locked implementation pipeline.

From a practical integration perspective, routine deployment requires attention to imaging availability, initialization robustness, runtime behavior, and case complexity. First, CBCT-derived condylar information materially improves THA-feasibility constraints; when high-quality condylar imaging is unavailable, a pragmatic fallback is to use population-informed condylar priors with uncertainty bounds and to flag such plans as lower-confidence for clinical review. Second, because THA estimation is sensitive to early landmarking/correspondence errors, quality-control gates (landmark plausibility checks, correspondence residual thresholds, and multi-start consistency checks) should be embedded before optimization acceptance. Third, the observed $\sim$18-second solve time is compatible with interactive digital planning: it is short enough for iterative parameter tuning during case setup, while still permitting repeated what-if evaluation in multidisciplinary planning sessions. Fourth, future extensions should explicitly model segmental osteotomies and asymmetry by adding segment-wise rigid transforms, side-specific constraint weights, and asymmetric correspondence masks, enabling the same framework to handle non-uniform surgical movements more faithfully.

Conclusion

The manuscript's primary contribution is a formal, reproducible optimization framework for mandibular arch coordination that integrates THA-referenced closure-path fidelity with Hawley–Bonwill posterior-geometry constraints in computational surgical planning.

The retrospective clinical component is intentionally reframed as a preliminary illustrative case series, and all empirical summaries are descriptive. No causal or comparative efficacy claim is made regarding Hawley–Bonwill planning from these data. The most relevant next step is prospective evaluation of the locked formulation and implementation pipeline in explicit, non-confounded planning groups.

References

[1] Bae, M., et al. (2025). 42° as a reference for modern orthodontic arch forms: A mathematical analysis of the Bonwill and Hawley methods. *Journal of Orofacial Orthopedics / Fortschritte der Kieferorthopädie*. https://doi.org/10.1007/s00056-025-00629-3

[2] Alkhayer, A., Piffkó, J., Lippold, C., Segatto, E., et al. (2020). Accuracy of virtual planning in orthognathic surgery: A systematic review. *Head & Face Medicine*.

[3] Hsu, S.-S., Gateno, J., Bell, R. B., et al. (2015). Virtual surgical planning for orthognathic surgery using digital data transfer and an intraoral fiducial marker (the Charlotte method). *Journal of Oral and Maxillofacial Surgery*.

[4] Chung, M., Lee, J., Song, W., Song, Y., Yang, I.-H., Lee, J., & Shin, Y.-G. (2019). Automatic registration between cone-beam CT and scanned surface via deep-pose regression neural networks and clustered similarities. *arXiv preprint*.

[5] The Glossary of Prosthodontic Terms. (latest ed.). Definitions of hinge axis and terminal hinge axis. *Journal of Prosthetic Dentistry*.